Effects of the Chirality and Functionality of Monomers on the Holographic Gratings Formed in Photosensitive Films

Jui-Hsiang Liu, Fuh-Tsang Wu

Department of Chemical Engineering, National Cheng Kung University, Tainan, 70101 Taiwan, Republic of China

Received 5 December 2002; accepted 11 March 2003

ABSTRACT: Photosensitive holographic polymer films were fabricated. Instead of liquid crystals, a nonreactive high-refractive-index diphenyl sulfide was mixed with several monomers and an initiator for the preparation of the holographic grating films. To investigate the formation of periodic arrays of the photosensitive refractive-index modulation films and the effects of the chirality and functionality of monomers on the diffraction efficiency, chiral monomeric (−)-bornyl acrylate, (+)-bornyl acrylate, and the racemate (±)-bornyl acrylate were synthesized and copolymerized with various multifunctional monomers. A reasonable schematic of the photosensitive polymerization mechanism was proposed. The effects of the multifunctional monomers, initiator concentrations, and feed monomer concentrations on the diffraction efficiencies were investigated. The morphologies of the polymer matrices were studied with scanning electron microscopy. Pictures of real light diffraction patterns with 15 grating points were obtained. In comparison with those described in the literature, the diffraction efficiency obtained in this investigation was relatively high. J Appl Polym Sci 90: 2246–2254, 2003

Key words: chiral; films; monomers

INTRODUCTION

A number of photopolymerizable systems have been proposed for recording phase holograms.[1,2] Under various conditions, both thin and volume holograms have been produced. It is possible to form holographic gratings in photopolymer systems in a single-step process at a relatively high speed.[3,4] The selection of different sensitizing dyes allows the use of several different optical recording wavelengths.[5] Several types of photopolymer systems for holographic recording have been reported.[6–9] Photopolymeric materials have the advantages of self-development, high angular selectivity, and high resolution, which make them more suitable for applications such as optical storage, holographic optical elements, optical computing, and holographic interferometry.[10–12]

The refractive-index modulation in photopolymer systems is due to the spatial density or concentration variations in the resulting polymer or spatially distributed voids. Similarly, when a liquid-crystal (LC)/monomer solution containing a photoinitiator is irradiated by a spatially periodic intensity, a grating of LC droplets will be formed. Optical gratings that exhibit multiple diffraction orders [the Raman–Nath (RN) regime] have been demonstrated in polymer-dispersed liquid-crystal (PDLC) films.[13,14]

The development of periodic arrays of PDLC droplets embedded in a polymeric matrix results in a refractive-index profile across the film leading to a diffraction of light. The ability to switch the effective refractive index of the LC domains allows us to control the diffraction of light from these structures. These structures can be formed on a variety of length scales ranging from the RN regime to the Bragg regime.

For chiral nematic LCs, the existence of a chiral compound will affect the orientation of LC molecules and lead to some specific arrangements. In another article, it has been reported that the steric hindrance and molecular arrangement of chiral segments affect the physical properties of photoresists.[15,16] In studying the steric effects on the diffraction efficiency (DE) of holographic grating films, we have synthesized a series of chiral monomers. For high DEs to be obtained, there must be a large refractive-index difference between the polymer-rich region and the inert-component-rich regions. Instead of LCs, in this investigation we have used a high-refractive-index diphenyl sulfide (DS; $n_D^{20} = 1.6327$) mixed with multifunctional monomers and an initiator to prepare holographic grating films. Moreover, to investigate the formation of the periodic arrays of the photosensitive refractive-index modulation films and the effects of chiral monomers on DE, we have synthesized chiral monomeric (−)-bornyl acrylate [(−)-BA] and (+)-bornyl acrylate [(+)-BA)] and the racemate (±)-bornyl acrylate [(±)-BA] and further blended them with various multifunc-

Correspondence to: J.-H. Liu (jhliu@mail.ncku.edu.tw).
Contract grant sponsor: National Science Council of Taiwan; contract grant number: NSC90-2216-E006-027.

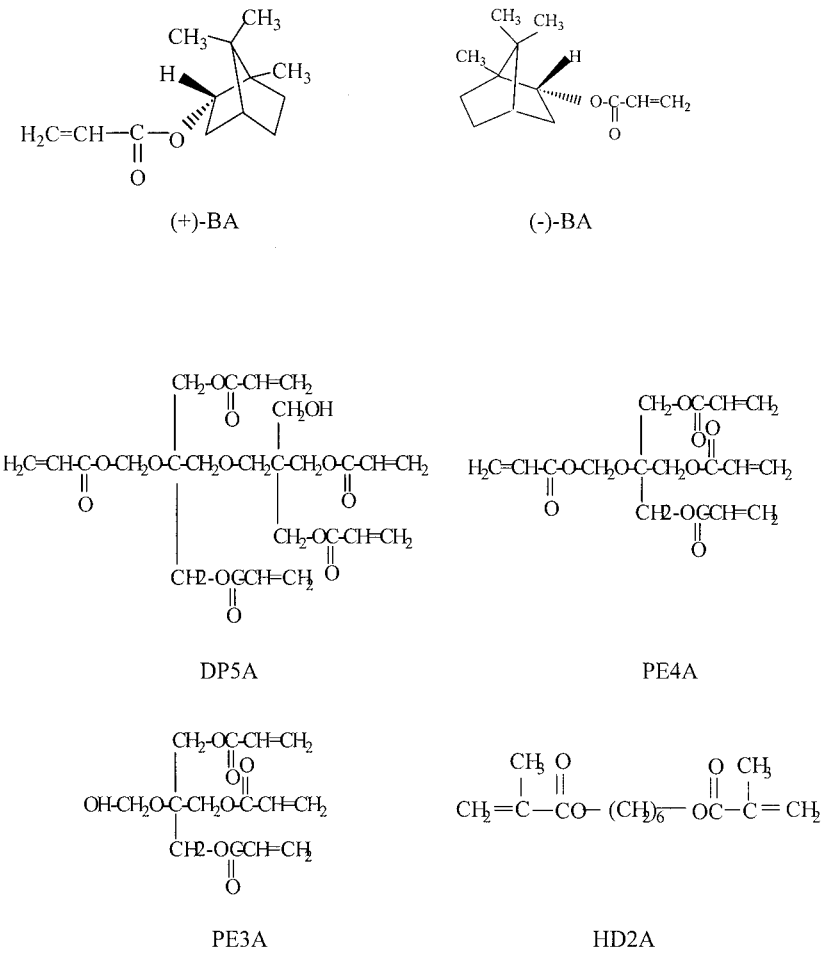

Scheme 1 Monomer structures.

tional monomers. We have studied the morphologies of the polymer matrices with scanning electron microscopy (SEM). A schematic mechanism of the photosensitive polymerization and the formation of grating arrays in polymer films are proposed.

EXPERIMENTAL

Materials

DS (n_D^{20} = 1.633) was purchased from TCI (Tokyo, Japan), and rose bengal bis(triethyl ammonium) salt (RB) and *N*-phenyl glycine (NPG) were obtained from Aldrich (Milwaukee, WI) and Acros (Geel, Belgium), respectively. Multifunctional monomers of dipentaerythritol pentaacrylate (DP5A), pentaerythritol tetraacrylate (PE4A), pentaerythritol triacrylate (PE3A), and 1,6-hexanediol dimethacrylate (HD2A) were purchased from Aldrich. Scheme 1 shows the structures of the compounds used in this investigation. (+)-Camphor, sodium metal, and ligroin, purchased from Wako Chemicals Co., Ltd. (Osaka, Japan), were extra pure-grade. Lithium aluminum hydride, silica gel, and organic solvents were acquired from Merck Co. (Darmstadt, Germany); petroleum benzine (bp = 50 –90°C) was obtained from Hayashi Co. (guarantied reagent-grade). The organic solvent was dehydrated by distillation over magnesium sulfate and then redistilled in the presence of sodium metal. The anhydrous solvent was kept in the presence of sodium.

Measurements

Fourier transform infrared (FTIR) spectra were recorded on a Jasco Valor III FTIR spectrophotometer (Tokyo, Japan). NMR spectra were obtained on a Bruker AMX-400 high-resolution NMR spectrometer (Germany). Optical rotations were measured at 30°C in dimethylformamide with a Jasco DIP-360 automatic digital polarimeter with readings to ±0.001°. Elemental analyses were conducted with a Heraeus CHN-O rapid elemental analyzer (Germany). Gel permeation chromatography measurements were carried out at 40°C on a Hitachi L-4200 instrument equipped with TSK gel (Tokyo, Japan) GMH and G2000H columns with tetrahydrofuran (THF) as an eluent. Chromatographic resolution was accomplished on a Hitachi

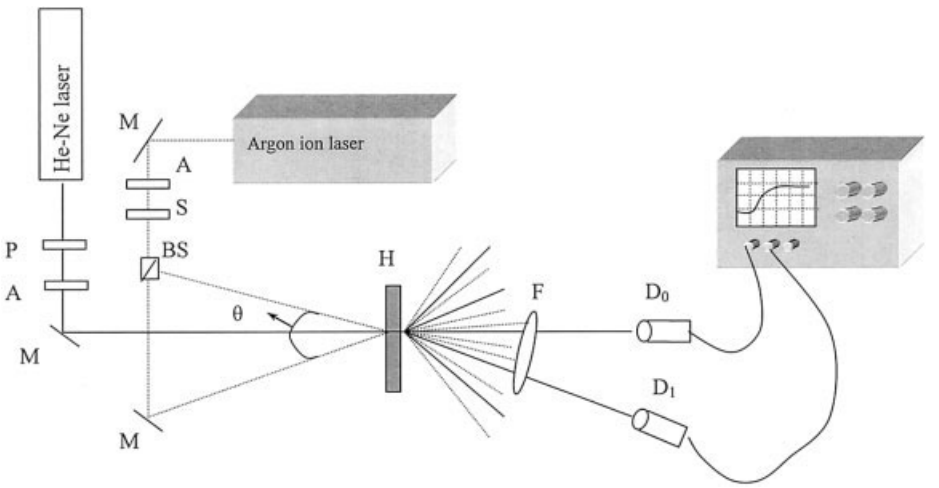

Scheme 2 Holographic recording and real-time optical reading experimental setup. BS = beam splitter; D = photodiode detector; M = mirror; H = holographic plate; S = shutter; P = polarizer; F = filter; A = attenuator.

L-6000 equipped with a Shimadzu C-R4A data processor (Osaka, Japan).

Synthesis of (+)-BA, (−)-BA, and (±)-BA

(+)-Borneol obtained from (+)-camphor by sodium metal oxidation was treated with acrylic acid to yield (+)-BA. Scheme 1 shows the molecular structures of the chiral monomers and achiral multifunctional monomers used in this investigation. The monomers synthesized in this investigation were identified with elemental analysis, FTIR, and NMR spectra. A typical method was as follows. A mixture of (+)-borneol (15.4 g), acrylic acid (36.03 g), and *p*-toluenesulfonic acid (2 g) was heated in 200 mL of benzene at 100°C in the presence of hydroquinone (2 g). Water, liberated during the reaction, was removed with a Dean–Stark apparatus for 20 h. After the completion of the reaction, the resulting mixture was washed with a dilute and aqueous sodium hydrogen carbonate solution and then with water. The oily layer was separated, dried over anhydrous magnesium sulfate, and distilled *in vacuo* to yield the product.

Yield: 67%. $[\alpha]_D^{25}$: +31.9° (c = 0.1 mg/dL, THF). FTIR (KBr, cm^{-1}): 2954, 2877 (CH), 1725 (C═O), 1636, 1618 (C═C). Mass: 208 g mol^{-1}. ^{1}H-NMR ($CDCl_3$, δ): 0.95 (s, 3H, CH_3), 1.02 (d, 6H, 7CH_3), 1.93 (d, 1H, 4H), 4.96 (m, 1H, 2-exo-H), 5.90, 6.15, 6.37 (each s, 3H, CH═CH_2). Elem. Anal. Calcd. for $C_{13}H_{20}O_2$ (208): C, 75.01%; H, 9.61%. Found: C, 75.05%; H, 9.58%.

Formation of the holographic grating films

A mixture of DP5A (4.3×10^{-1} g), RB (1.9×10^{-3} g), NPG (8.7×10^{-4} g), (−)-BA (1.6×10^{-1} g), and DS was poured into a glass cell with a 50-μm gap. The cell was irradiated with a 488-nm argon-ion laser for a certain period. After that, postcuring with a table light for 24 h was performed. The holographic grating film was then analyzed with the equipment shown in Scheme 2.

Analysis apparatus for DE

Real-time measurements of DE for transmission holograms were carried out with the system shown in Scheme 2. The holographic gratings were created with an argon-ion laser with a 488-nm wavelength that went through a beam splitter to split the light into two parts; the beam ratio was 1:1. The writing beams intersected in the sample film at an incident angle of $\theta/2 \sim 1.43°$, and this led to the formation of a grating with a fringe spacing of 9.8 μm. They were unfocused, each having a beam diameter of approximately 5 mm. The diffracted intensity was monitored with a helium–neon laser with a 633-nm wavelength, at which the material did not absorb. The intensity of the initial incident beam (I_0) was detected by the first photodiode detector (D_0), and that of the first-order diffracted beam (I_1) was detected by a second photodiode detector (D_1), both detectors being connected to an oscilloscope (2.5 samples/s). The first-order DE was defined as the intensity of light diffracted into the first order referenced to the total incoming light intensity:

$$\mathrm{DE} = \frac{I_1}{I_0} \tag{1}$$

After laser exposure, samples were allowed to be fully cured under a 28-W table light for 24 h. Fully cured samples showed no coloration because RB was completely bleached in the photocuring process.

The morphology of a cured grating array was examined with SEM. A sample was cut from an inter-

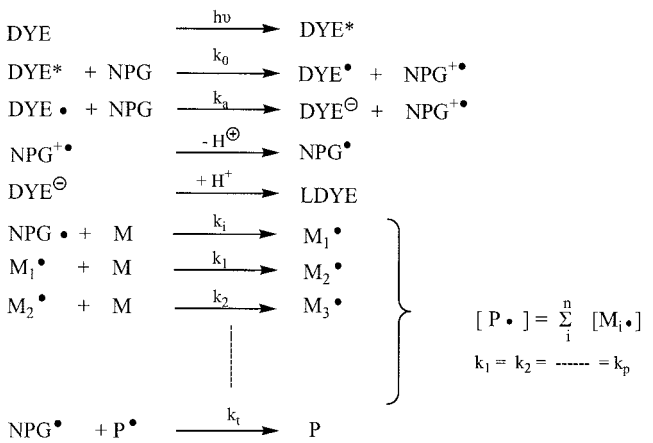

Scheme 3 Mechanism of photopolymerization.

section, submerged into *n*-hexane, and washed supersonically for 2 h. The unreacted monomer and inert component were then extracted, dried *in vacuo*, and coated with a gold film.

RESULTS AND DISCUSSION

To investigate the steric effects on DE, we synthesized chiral (+)-BA and (−)-BA and the racemate (±)-BA. Scheme 1 shows the mirror images of the enantiomers of bornyl acrylate. The multifunctional monomers shown in Scheme 1 were used to investigate the effect of the polymerization rate on DE. In general, the polymerization rate rises with an increasing number of functional groups of monomers. To initiate the polymerization of the monomers, we used RB and NPG as a photoinitiator and a coinitiator, respectively. The mechanism of photopolymerization is shown in Scheme 3. RB was excited by laser light, and then the eximer transmitted its energy to the coinitiator to generate the active sites, at which point the photopolymerization was initiated.

To prepare the grating array membrane, we poured a mixture of DP5A, RB, NPG, and DS into a glass cell with a 50-μm gap. The cell was exposed to a 488-nm argon-ion laser for a certain period. After that, it was postcured with a table light for 24 h. Scheme 4 shows the occurrence of phase separation during laser exposure, which led to the formation of the grating patterns. Before laser irradiation, the monomer mixture was a homogeneous liquid. The laser interference pattern was recorded on the polymer membrane after sufficient laser irradiation and postirradiation by a table light. As can be seen in Scheme 4(b), high energy irradiation could cause the initiation of monomer polymerization. Nonreactive DS was pushed to the other sides; at the same time, the monomers continued to diffuse to the high-energy-irradiated region, and this led to the formation of the grating arrays.

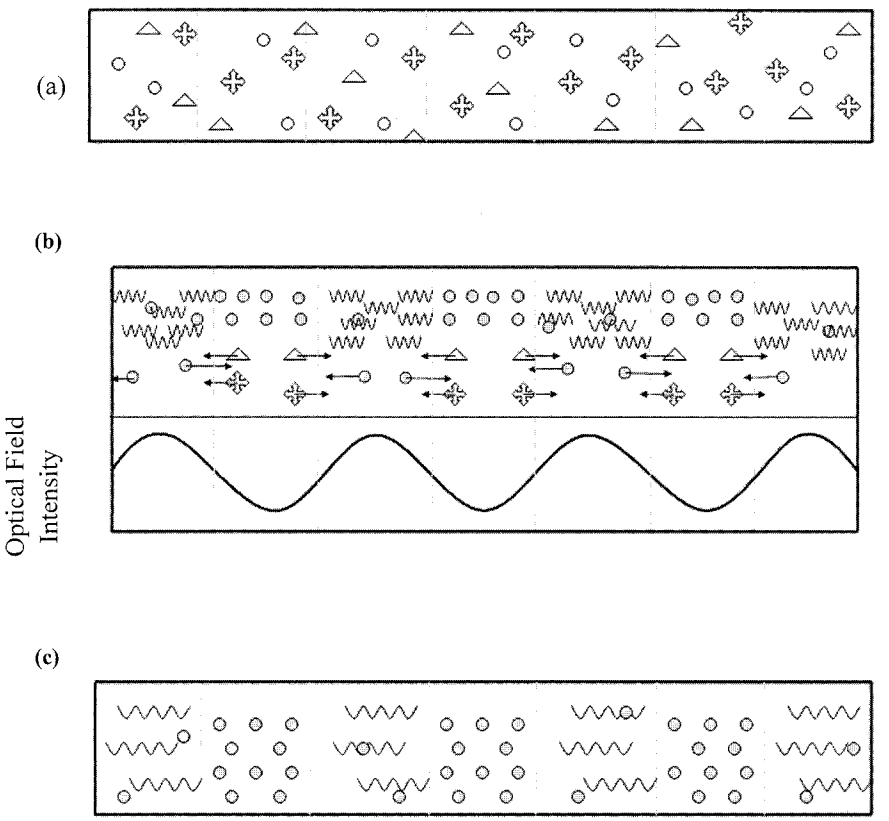

Scheme 4 Phase separation occurring in the membrane (a) before, (b) during, and (c) after laser exposure.

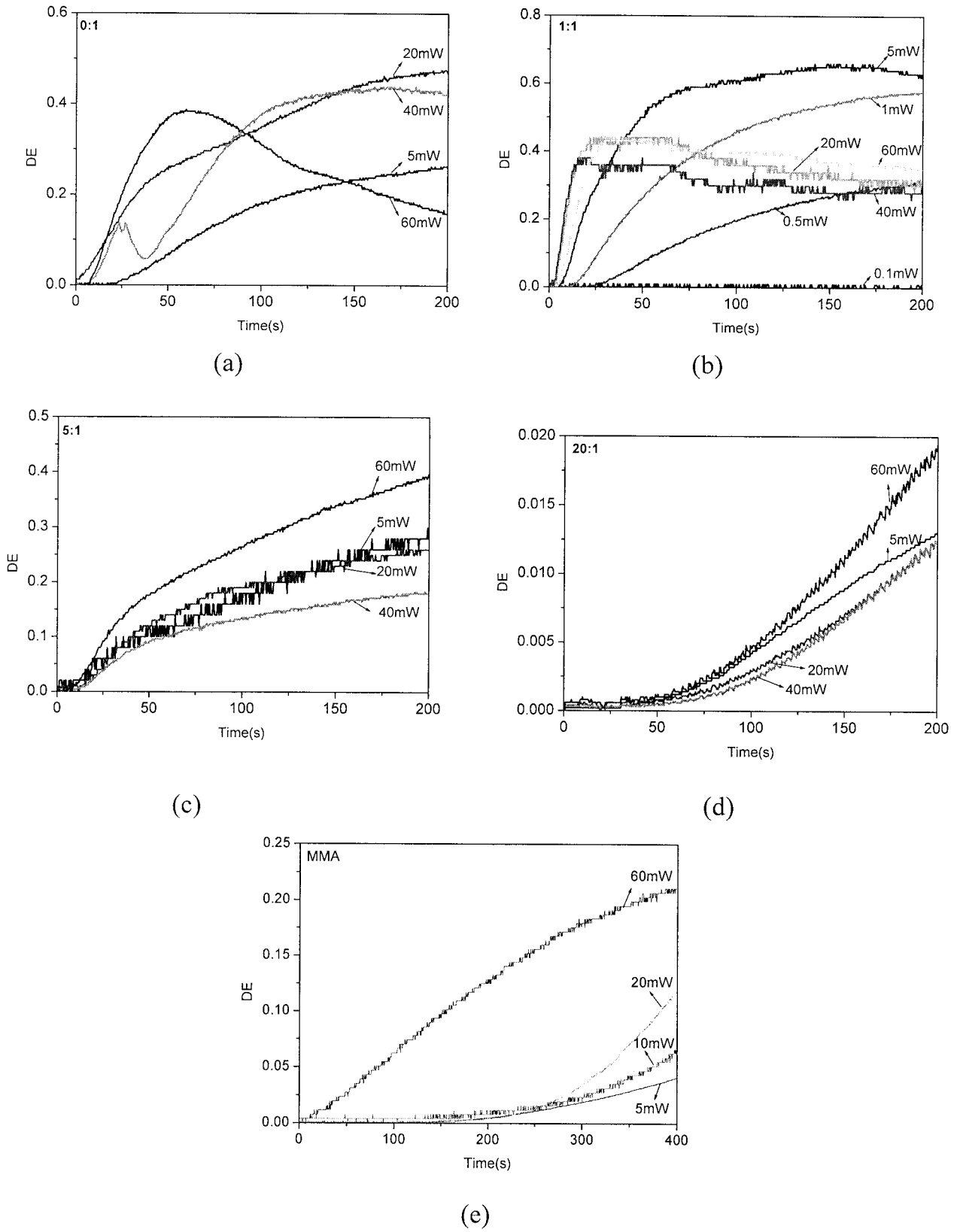

Figure 1 Effects of the chiral monomers on DE with various molar ratios in the presence of 0.1 mol % RB and 0.3 mol % NPG: (a) 0:1 (−)-BA/DP5A, (b) 1:1 (−)-BA/DP5A, (c) 5:1 (−)-BA/DP5A, (d) 20:1 (−)-BA/DP5A, and (e) 5:1 MMA/DP5A.

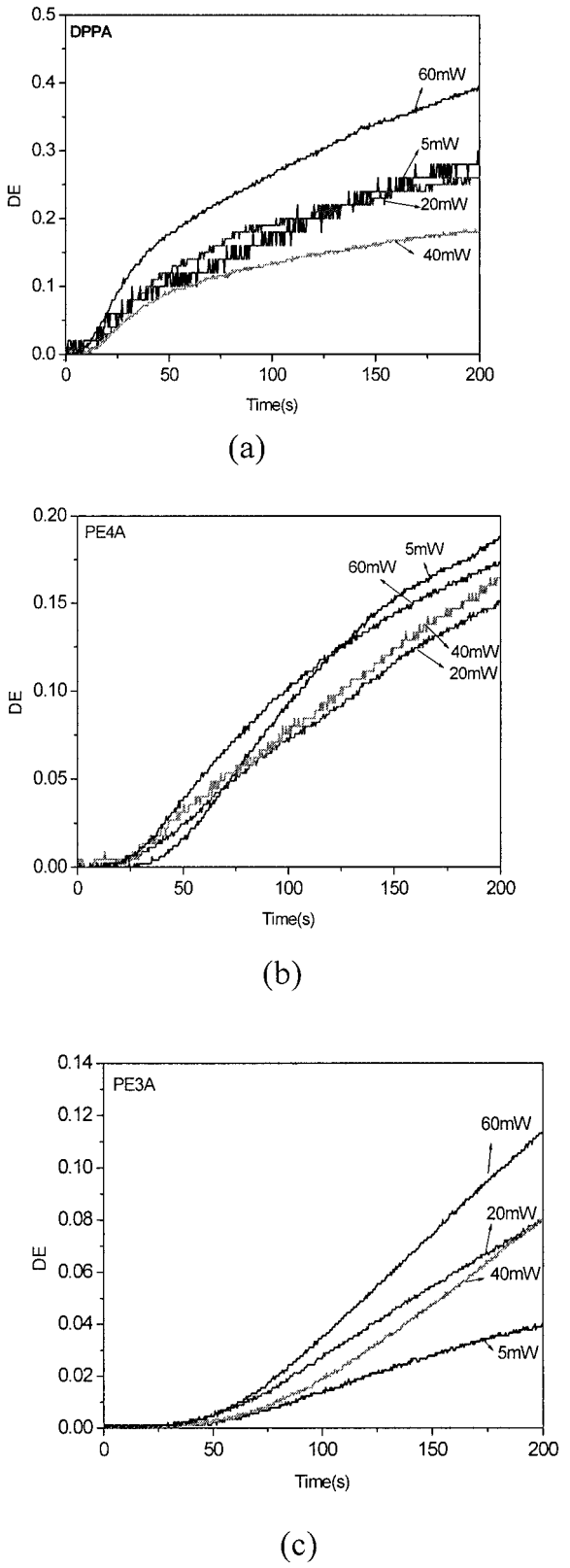

Figure 2 Dependence of the monomer functionality on DE with various incident light powers for (a) DP5A, (b) PE4A, and (c) PE3A in the presence of 0.1 mol % RB, 0.3 mol % NPG, and 5:1 multifunctional monomer/(−)-BA.

In investigating the steric effects of chiral monomers on DE, we mixed chiral (−)-BA with various amounts of DP5A and compared it to the achiral methyl methacrylate (MMA) system. As shown in Figure 1,

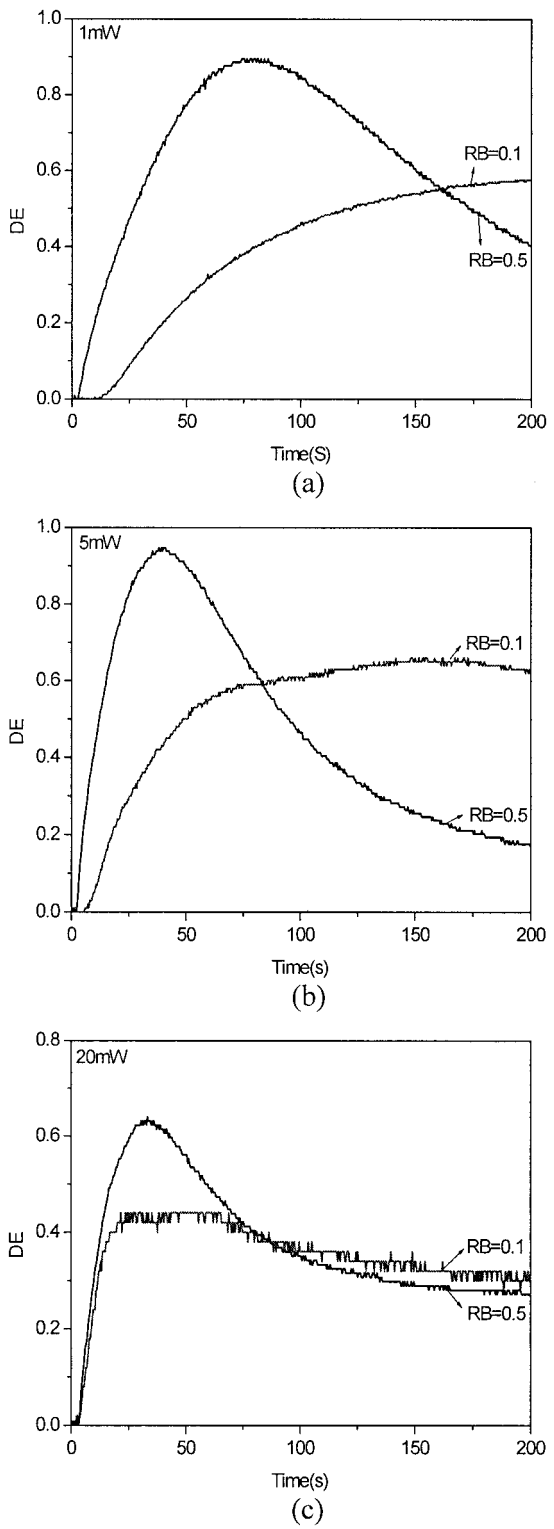

Figure 3 Effects of the initiator concentration on DE with various incident light powers in the presence of 1:3 RB/NPG: (a) 1, (b) 5, and (c) 20 mW.

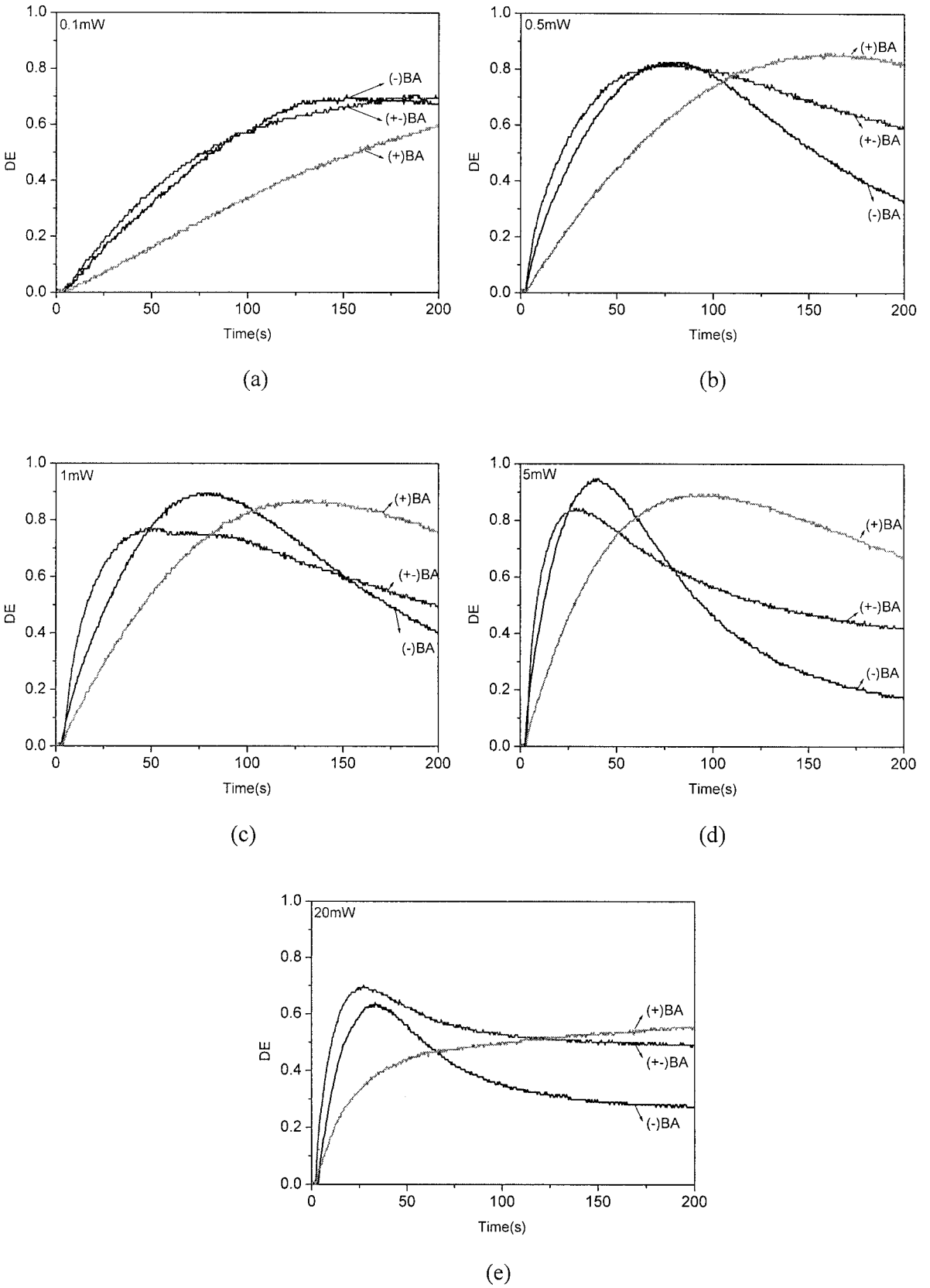

Figure 4 Effect of the chirality on DE with various light strengths in the presence of 0.5 mol % RB and 1.5 mol % NPG: (a) 0.1, (b) 0.5, (c) 1, (d) 5, and (e) 20 mW.

TABLE I
Comparison of Various Photosensitive Grating Membranes

Material	Monomeric composition	Thickness (μm)	Wavelength (nm)	Sensitivity (mJ/cm^2)	Spatial resolution	Diffraction efficiency (%)	Reference
DuPont's HRF-700X		10–20	476–532	3–30	—	>99	18
DuPont's Omnidex 7061		20	476–532	25	—	>99	19
From Tomlinson et al.	Mixture of methacrylates	2000	325	50–150	5,000	70	10
From Calixto	Acrylamide	40	633	94	100	10	20
From Boiko et al.	Acrylamide	100	1,060	94	10	55	21
From Fuh et al	Acrylate, LC	36	514	40	100	40	22
From Ichimura et al.	Azo acrylate, LC	25	436	10,000	560	0.026	23
Our system	Mixture of acrylates	50	488	150	100	80	

the light exposure strength had obvious effects on the polymerization of the monomers and the separation of the polymers. The maximum DE of 0.65 is shown in Figure 1(b). Figure 1(c,e) shows that the polymerization rate and the efficiency of phase separation of the (−)-BA system were higher than those of the MMA system, and this led to an increase in DE. In principle, the relationship between (−)-BA and MMA is diastereomeric; that is, they have different physical properties, including the polymerization rate, phase-separation rate, solubility for DS, and even refractive index.

The effect of multifunctional monomers on DE is shown in Figure 2. Monomers with various amounts of functional groups were mixed with certain amounts of (−)-BA. As shown in Figure 2(a), DE increased with increasing amounts of the functional groups existing in the monomers. The polymerization rate of the monomers could accelerate with an increasing number of the functional groups. Higher functioning monomers could also increase the matrix density and lead to a greater difference of the refractive index (Δn) between grating arrays. In theory, DE of the RN regime can be represented by the following equation:[1,2,17]

$$\eta = \left(\frac{\pi \Delta \tilde{n} d}{\lambda}\right)^2 \tag{2}$$

where d is the film thickness and $\Delta\tilde{n}$ represents the degree of change in the complex refractive index. A high DE value is obtained when there is a large $\Delta\tilde{n}$ value between the polymer-rich region and the inert-component-rich region. As mentioned previously, DE is governed by three parameters: $\Delta\tilde{n}$, λ, and d. In this case, λ and d were 488 nm and 50 μm, respectively. Consequently, such a difference in the diffraction would only be related to $\Delta\tilde{n}$.

As shown in Scheme 3, the decomposition of the initiator caused monomer polymerization. Figure 3 shows the effects of the initiator on DE of the grating membrane. A higher initiator content system resulted in more rapid phase separation and an excellent value of DE. A DE of 0.95 was achieved, as shown in Figure 3(b). With 20-mW laser irradiation, the optimal value could be achieved within 30 s. The effects of various power strengths from the light source can also be seen in the figure. The results suggested that the polymerization rate and phase separation could rise with the increasing generation of light-induced active sites. Both a higher initiator concentration and a higher degree of stronger light accelerated the formation of grating patterns and Δn, leading to increases in DE. Figure 3(c), however, shows that an overly high degree of light could cause the polymerization to occur in a short time, inhibiting the interflow between DS and the monomers and leading to a notable decrease in DE.

In theory, enantiomers have the same physical properties, including the polymerization rate. The existence of achiral multifunctional monomers, however, changes the relationship of polymers from enantiomeric to diastereomeric. Figure 4 shows the dependence of first-order DE on the laser irradiation time for diastereomeric (+)-BA, (−)-BA, and (±)-BA with various light strengths. Diastereomeric polymers, as mentioned previously, have different polymerization rates, mobility values, and even refractive indices, which lead to different dynamic behaviors. As shown in Figure 4, membranes containing (+)-BA could reduce the polymerization rate. (−)-BA showed relatively higher DEs and phase-separation rates. A DE of around 95% was achieved for (−)-BA with a 5-mW laser. The light power effect can also be seen in this figure; the results are similar to those described in Figure 3. For this system, the maximum value was achieved in Figure 4(d).

Table I compares the physical properties of photosensitive membranes discussed in the literature and in

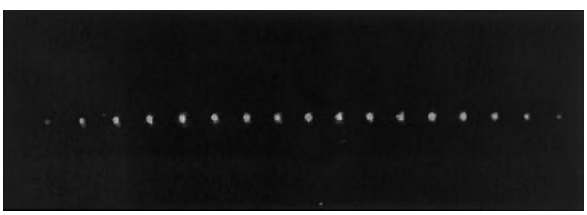

Figure 5 Real diffraction pattern of laser light through a grating spot recorded on a membrane with 1:1 (−)-BA/DP5A, 0.5 mol % RB, and 1.5 mol % NPG.

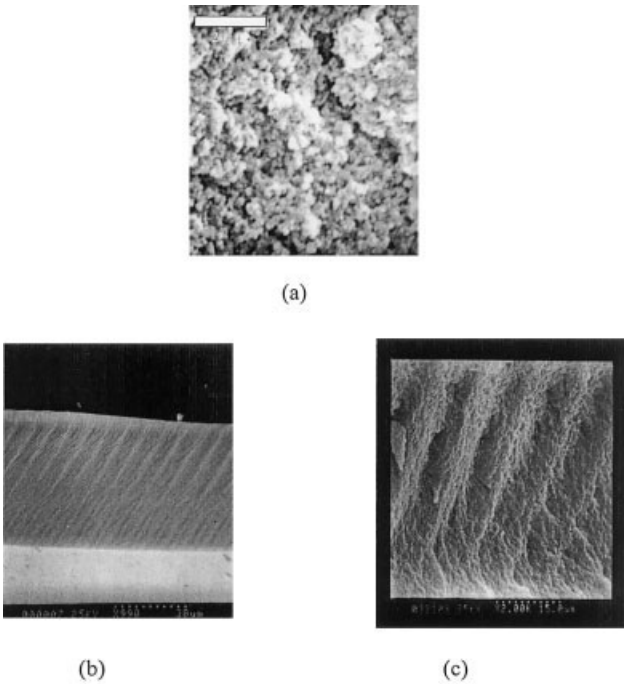

Figure 6 SEM micrographs of the cross section of a grating membrane: (a) the morphology of the polymer matrix, (b) a film exposed for 20 s, and (c) a film sufficiently exposed to a laser.

this investigation. In our system, nonreactive DS was used instead of traditional anisotropic LCs. The DE obtained in our investigation showed a relatively higher value. Figure 5 shows the real diffraction pattern of laser light through a grating spot recorded on a membrane with 1:1 (−)-BA/DP5A in the presence of 0.5 mol % RB and 1.5 mol % NPG. As shown in the figure, a composite film could be recorded as the RN grating with a small incident writing angle.

Figure 6 shows the morphology of a grating membrane with a side-view SEM image. As shown in Figure 6(a), the polymer-rich fringe with a porous structure means that some DS molecules were trapped in the network during polymerization. Figure 6(b) shows the variation of grating as a function of depth. Because the writing beams were irradiated from the top surface of the film, in this case, after a short period of laser writing, the film was then exposed to a table light. A homogeneous fringe array can be seen in the upper side of the film, but a homogeneous polymer matrix without any grating was formed in the second stage of table-light exposure. Figure 6(c) shows an SEM micrograph of the cross section of the grating membrane reported in Figure 5. Different contents of DS in the polymer matrix between the fringe arrays caused the formation of Δn, which led to the occurrence of light grating through the films.

CONCLUSIONS

Holographic grating membranes were fabricated with nonreactive DS with (+)-BA, (−)-BA, and (±)-BA and multifunctional monomers in the presence of a photoinitiator. Relatively higher DE grating membranes were obtained. The holographic properties were confirmed by real light grating through spots recorded on the membranes. From SEM micrographs of membrane cross sections, the existence of a periodic grating array was established. High-refractive-index DS was found to be useful for the fabrication of holographic grating membranes.

References

1. Hariharan, P. Optical Holography: Principles, Techniques and Applications; Cambridge University Press: Cambridge, England, 1984.
2. Eichler, H. J.; Gunter, P.; Pohl, D. W. Laser-Induced Dynamic Gratings; Springer-Verlag: Berlin, 1986.
3. Das, P. Lasers and Optical Engineering; Springer-Verlag: New York, 1991.
4. Gunter, P.; Huignaed, J. P. Photorefractive Materials and Their Applications; Springer-Verlag: Berlin, 1989.
5. Ohe, Y.; Ito, H.; Watanabe, N.; Ichimura, K. J Appl Polym Sci 2000, 7, 2189.
6. Fuh, A. Y. G.; Huang, C. Y.; Tsai, M. S.; Chen, J. M.; Chien, L. C. Jpn J Appl Phys 1996, 35, 630.
7. Fuh, A. Y. G.; Tsai, M. S.; Huang, C. Y.; Ko, T. C. Opt Quantum Electron 1996, 28, 1535.
8. Sutherland, R. L.; Natarajan, L. V.; Tondiglia, V. P.; Bunning, T. J. Chem Mater 1993, 5, 1533.
9. Blaya, S.; Carretero, L.; Mallavia, R.; Fimia, A.; Madrigal, R. F.; Ulibarrena, M.; Levy, D. Appl Opt 1998, 37, 7604.
10. Tomlinson, W. J.; Chandross, E. A.; Weber, H. P.; Aumiller, G. D. Appl Opt 1976, 15, 534.
11. Fuh, A. Y. G.; Ko, T. C.; Tsai, M. S.; Huang, C. Y. J Appl Phys 1998, 83, 679.
12. Fuh, A. Y. G.; Tsai, M. S.; Lee, C. R.; Fan, Y. H. Phys Rev E 2000, 62, 3702.
13. Caputo, R.; Sukhov, A. V.; Tabiryan, N. V.; Umeton, C. Chem Phys 1999, 245, 463.
14. Bunning, T. J.; Natarajan, L. V.; Tondiglia, V. P.; Sutherland, R. L. Annu Rev Mater Sci 2000, 30, 83.
15. Pogue, R. T.; Sutherland, R. L.; Schmitt, M. G.; Natarajan, L. V.; Swecki, S. A.; Tondiglia, V. P.; Bunning, T. J. Appl Spectrosc A 2000, 54, 12.
16. Kogelink, H. Bell Syst Tech J 1969, 48, 2909.
17. Pogue, R. T.; Natarajan, L. V.; Siwecki, S. A.; Tondiglia, V. P.; Sutherland, R. L.; Bunning, T. J. Polymer 2000, 41, 733.
18. Gambogi, W. J., Jr.; Steijn, K. W.; Mackara, S. R.; Duzick, T.; Kelly, J. Proc SPIE 1994, 2152, 282.
19. Stevenson, S. H.; Armstrong, M. L.; O'Connor, P. J.; Tipton, D. F. Proc SPIE 1995, 2333, 60.
20. Calixto, S. Appl Opt 1987, 26, 3904.
21. Boiko, Y. B.; Solovjer, V. S.; Calixto, S.; Lougnot, D. J. Appl Opt 1994, 33, 787.
22. Fuh, A. Y. G.; Tsai, M. S.; Huang, L. J.; Liu, T. C. Appl Phys Lett 1999, 74, 2572.
23. Yoshimoto, N.; Morino, S.; Nakagawa, M.; Ichimura, K. Opt Lett 2002, 27, 182.